IRAQI JOURNAL OF APPLIED PHYSICS

The *Iraqi Journal of Applied Physics (IJAP)* is a peer reviewed journal of high quality devoted to the publication of original research papers from applied physics and their broad range of applications. IJAP publishes quality original research papers, comprehensive review articles, survey articles, book reviews, dissertation abstracts in physics and its applications in the broadest sense. It is intended that the journal may act as an interdisciplinary forum for Physics and its applications. Innovative applications and material that brings together diverse areas of Physics are particularly welcome. Review articles in selected areas are published from time to time. It aims to disseminate knowledge; provide a learned reference in the field; and establish channels of communication between academic and research experts, policy makers and executives in industry, commerce and investment institutions. IJAP is a quarterly specialized periodical dedicated to publishing original papers, letters and reviews in: Applied & Nonlinear Optics, Applied Mechanics & Thermodynamics, Digital & Optical Communications, Electronic Materials & Devices, Laser Physics & Applications, Plasma Physics & Applications, Quantum Physics & Spectroscopy, Semiconductors & Optoelectronics, Solid State Physics & Applications, Alternative and Renewable Energy, and Computers and Networks.

ISSN (Print): 1813-2065, ISSN (Online): 2309-1673, ISSN (Letters): 1999-656X

EDITORIAL BOARD

Editorial Office:
P. O. Box 55259, Baghdad 12001, IRAQ
Website: www.iraqiphysicsjournal.com
Emails: info@iraqiphysicsjournal.com, editor_ijap@yahoo.co.uk, editor@ijaponline.com

ADVISORY BOARD

SPONSORED AND PUBLISHED BY
THE IRAQI SOCIETY FOR ALTERNATIVE AND RENEWABLE ENERGY SOURCES & TECHNIQUES (I.S.A.R.E.S.T.)

IRAQI JOURNAL OF APPLIED PHYSICS

ISSN (Print): 1813-2065, ISSN (Online): 2309-1673, ISSN (Letters): 1999-656X

" INSTRUCTIONS TO AUTHORS "

CONTRIBUTIONS

Contributions to be published in this journal should be original research works, i.e., those not already published or submitted for publication elsewhere, individual papers or letters to editor.
Manuscripts should be submitted to the editor at the mailing address:
Iraqi Journal of Applied Physics, Editorial Board, P. O. Box 55259, Baghdad 12001, IRAQ
Website: www.iraqiphysicsjournal.com
Email: editor@iraqiphysicsjournal.com, editor_ijap@yahoo.co.uk

MANUSCRIPTS

Two hard copies with soft copy on a compact disc (CD) should be submitted to Editor in the following configuration:

- **One-column** Double-spaced one-side A4 size with 2.5 cm margins of all sides
- Times New Roman font (16pt bold for title, 14pt bold for names, 12pt bold for headings, 12pt regular for text)
- Letters should not exceed 10 pages, papers should not exceed 20 pages and reviews are up to author.
- Manuscripts presented in English only are accepted.
- English abstract not exceed 150 words
- 4 keywords (at least) should be maintained on (PACS preferred)
- Author(s) should express all quantities in SI units
- Equations should be written in equation form (*italic* and symbolic)
- Figures and Tables should be separated from text
- Figures and diagrams can be submitted in colors for assessment and they will be returned to authors after provide printable copies
- Charts should be indicated by the software used for
- Only original or high-resolution scanner photos are accepted
- For electronic submission, articles should be formatted with MS-Word software.

AUTHOR NAMES AND AFFILIATIONS

It is IJAP policy that all those who have participated significantly in the technical aspects of a paper be recognized as co-authors or cited in the acknowledgments. In the case of a paper with more than one author, correspondence concerning the paper will be sent to the first author unless staff is advised otherwise.
Author name should consist of first name, middle initial, last name. The author affiliation should consist of the following, as applicable, in the order noted:
- Company or college (with department name or company division), Postal address, City, state, zip code, Country name, contacting telephone, and e-mail

REFERENCES

The references should be brought at the end of the article, and numbered in the order of their appearance in the paper. The reference list should be cited in accordance with the following examples:
[1] X. Ning and M.R. Lovell, "On the Sliding Friction Characteristics of Unidirectional Continuous FRP Composites", *ASME J. Tribol.*, 124(1) (2002) 5-13.
[2] M. Barnes, "Stresses in Solenoids", *J. Appl. Phys.*, 48(5) (2001) 2000–2008.
[3] J. Jones, **"Contact Mechanics"**, Cambridge University Press (Cambridge, UK) (2000), Ch.6, p.56.
[4] Y. Lee, S.A. Korpela and R. Horne, "Structure of Multi-Cellular Natural Convection in a Tall Vertical Annulus", Proc. 7th International Heat Transfer Conference, U. Grigul et al., eds., Hemisphere (Washington DC), 2 (1982) 221–226.
[5] M. Hashish, "Waterjet Technology Development", High Pressure Technology, PVP-Vol. 406 (2000) 135-140.
[6] D.W. Watson, "Thermodynamic Analysis", ASME Paper No. 97-GT-288 (1997).
[7] C.Y. Tung, "Evaporative Heat Transfer in the Contact Line of a Mixture", Ph.D. thesis, Rensselaer Polytechnic Institute, Troy, NY (1982).

PROOFS

Authors will receive proofs of papers and are requested to return one corrected hard copy with a WORD copy on a compact disc (CD). New materials inserted in the original text without Editor permission may cause rejection of paper.

COPYRIGHT FORM

Author(s) will be asked to transfer copyrights of the article to the Journal soon after acceptance of it. This will ensure the widest possible dissemination of information.

OFFPRINTS

Authors will receive offprints free of charge and any additional reprints can be ordered.

SUBSCRIPTION AND ORDERS

Annual fees (4 issues per year) of subscription are:
50 US$ for individuals inside Iraq; **200** US$ for institutions inside Iraq;
100 US$ for individuals abroad; **300** US$ for institutions abroad.
Fees are reduced by 25% for I.S.A.R.E.S.T. members. Orders of issues can be submitted by contacting the editor-in-chief or editorial office at admin@iraqiphysicsjournal.com, or editor_ijap@yahoo.co.uk to maintain the address of issue delivery and payment way.

Appreciation to

Professor Franko Küppers

for his contribution to IJAP as Advisory Board Member since 2005

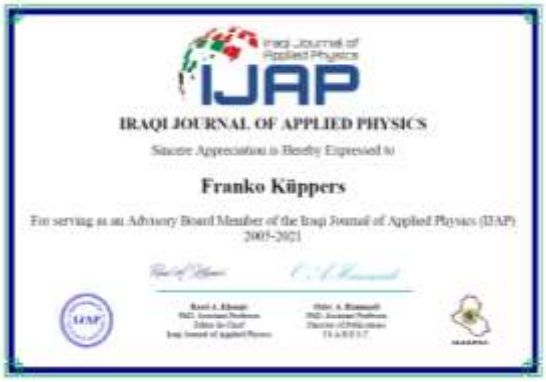
IRAQI JOURNAL OF APPLIED PHYSICS

Sincere Appreciation is Hereby Expressed to

Franko Küppers

For serving as an Advisory Board Member of the Iraqi Journal of Applied Physics (IJAP)
2005-2021

Speaking on behalf of the authors, readers, and editorial board members of Iraqi Journal of Applied Physics (IJAP), I would like to express my deep gratitude for Professor Franko Küppers, Director of the Skoltech Center for Photonics and Quantum Materials, Skoltech faculty, Russia for his valuable contribution as an advisory board member since 2005. The time and effort invested into the review process by the members of the Advisory Board makes it possible for IJAP to publish high-quality research. I am particularly appreciative of the valuable contributions that advisory board members have made to IJAP despite the numerous difficulties in education and research due to coronavirus disease 2019 (COVID-19). It is a nice opportunity to introduce Professor Küppers for IJAP readers.

Franko Küppers, Fellow of SPIE and Senior Member of the IEEE photonics and communications section, was with Siemens and with Deutsche Telekom's Research and Technology Center where he directed the Optical Networks research group and the Photonic Systems department until 2002.

In 2003, he joined the College of Optical Sciences at the University of Arizona, where he served as a tenured Associate Professor, built and ran the Photonic Telecommunication Systems research group, and served as the testbed lead for the US National Science Foundation's Engineering Research Center for Integrated Access Networks (ERC CIAN) with which he is still associated as an Adjunct Professor.

In 2011, he joined the Institute for Microwave Engineering and Photonics at Darmstadt University of Technology (TU Darmstadt), Germany, where he also held the Chair of Photonics and Optical Communications and served as the Institute Director. He published more than 200 scientific articles and was a Guest Editor of the JLT Special Issue on 40 Gb/s Lightwave Systems in 2002. He received the US National Science Foundation CAREER Award, the Science Foundation Arizona Competitive Advantage Award, and the College Award of Distinction for Outstanding Undergraduate Teaching.

Since January 2019, he is with the Skolkovo Institute of Science and Technology, Moscow, Russia, as a Professor and Director of the Center for Photonics and Quantum Materials.


EDITORIAL BOARD

ADVISORY BOARD

The Editorial Board of IJAP are pleased to present the Certificate of Appreciation to Professor Franko Küppers to acknowledge his contributions. I would also like to express our appreciation to all of our members, and I hope that they will continue to provide unstinting support for the international community of science.

Thank you so much, Franko

Raad A. Khamis, PhD
Editor-In-Chief, IJAP

IRAQI JOURNAL OF APPLIED PHYSICS
Vol. 17, No. 2, April-June 2021, p. 4

Plasmon-Coupled Gold Nanoparticles Could be Used in Optical Thermal-History Sensor

Researchers have demonstrated that stretching shape-memory polymers embedded with clusters of gold nanoparticles alters their plasmon-coupling, giving rise to desirable optical properties. One potential application for the material is a sensor that relies on optical properties to track an object or environment's thermal history.

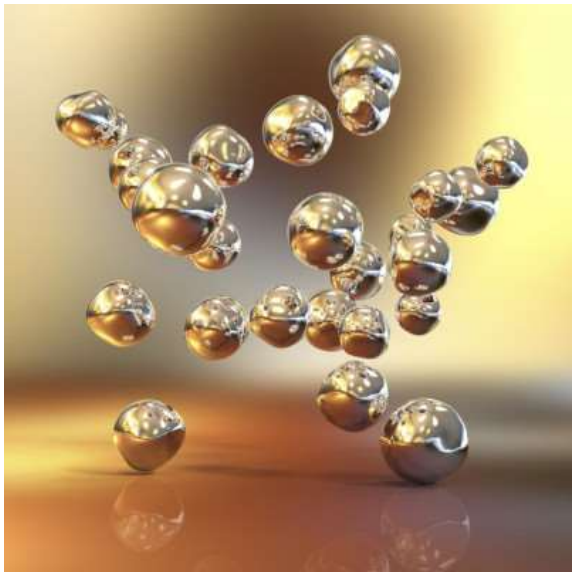

At issue is a stretchable polymer embedded with gold nanospheres. If the material is heated and stretched, followed by cooling to room temperature, the material will hold its stretched shape indefinitely. Once reheated to 120 degrees Celsius, the material returns to its original shape.

But what's really interesting is that the gold nanospheres are not perfectly dispersed in the polymer. Instead, they form clusters, in which their surface plasmon resonances are coupled.

These plasmon-coupled nanoparticles have optical properties that shift depending on how close they are to each other, which changes when stretching alters the shape of the composite.

"When assessing the peak wavelength of light absorbed by the material, there are significant differences depending on whether the light is polarized parallel or perpendicular to the stretching direction," says Joe Tracy, corresponding author of a paper on the work and a professor of materials science and engineering at NC State.

"For light polarized parallel to the direction of stretching, the further you have stretched the material, the further the light absorbed shifts to the red. For light polarized perpendicular to the stretching direction there is a blueshift."

"We also found that, while the shape-memory polymer holds its shape at room temperature, it recovers its original shape in a predictable way, depending on the temperature it is exposed to," says Tobias Kraus, co-author of the paper, a group leader at the Leibniz Institute for New Materials and a professor at Saarland University.

Specifically, once stretched 140% past its original length, you can determine the highest temperature to which the polymer is then exposed, up to 120 degrees Celsius, by measuring how much it has shrunk back toward its original size. What's more, because of the plasmon-coupled nanoparticles, this change can be measured indirectly, through measurements of the material's optical properties.

"From a practical perspective, this allows you to create an optical thermal-history sensor," Joe Tracy says. *"You can use light to see how hot the material got. An important application of thermal-history sensors is assuring the quality or safety of shipping or storing materials that are sensitive to significant changes in heat. We have demonstrated an approach based on plasmon coupling of gold nanoparticles."*

The sensor concept was developed empirically, but the researchers also used computational modeling to better understand the structure of the clusters of gold nanospheres and how the clusters changed during stretching. The strength of plasmon coupling is related to the spacings between nanospheres, which is known as a "plasmon ruler."

"Based on our simulations, we can estimate the distance between plasmon-coupled nanoparticles from their optical properties," says Amy Oldenburg, co-author of the paper and a professor of physics at the University of North Carolina at Chapel Hill. *"This comparison is informative for designing future polymer nanocomposites based on plasmon-coupled nanoparticles."*

The paper, "*Plasmon-Coupled Gold Nanoparticles in Stretched Shape-Memory Polymers for Mechanical/Thermal Sensing*," appears in the journal *ACS Applied Nano Materials*. First author of the paper is Prachi Yadav, a former graduate student at NC State. The paper was co-authored by Mehedi Rizvi, Sumeet Mishra, Brian Chapman and Brian Lynch of NC State; and Björn Kuttich of the Leibniz Institute for New Materials.

IRAQI JOURNAL OF APPLIED PHYSICS
Vol. 17, No. 2, April-June 2021, pp. 5-9

Effect of Average Ionic Radius of A-site, B-site in ABO_3 Perovskite Ceramics on Their Crystal Structures and Curie's Temperature

Jassim M. Yaseen

Department of physics, College of Education, Al-Iraqia University, Baghdad, IRAQ

Barium titanate ($BaTiO_3$) is one of the most ferroelectrics. It's commonly used in capacitors due to its high dielectric constant. In this study, our goal is to determine the extent to which the change in the average ionic radius of A, B sites affects the structural, dielectric properties of this ceramic. In this study, barium titanate ($Ba_{0.85}X_{0.15}TiO_3$, $BaY_{0.15}Ti_{0.85}O_3$) (X = Pb, Ca, Co, Y= Zr, Si, Mn) was prepared by solid state reaction method in which the calcination temperature was 1200 °C for 2 hours. Structural characterization and dielectric properties were determined and calculated by using x-ray diffractometer, RCL-Meter (PM6303) at frequency 20 Hz using different temperature respectively. The results of the work showed that the average ionic radius at the A, B sites plays a large and clear role in determining the values of the dielectric constant and Curie temperature in perovskites in addition to the structural parameters.

Keywords: Ceramic; Crystal structure; Perovskite; Crystallographic structure
Received: 12 April 2021; **Revised:** 5 May 2021; **Accepted:** 12 May 2021

1. Introduction

Barium titanate ($BaTiO_3$) is one of the most common ferroelectrics. Ferroelectricity is the spontaneous polarization in the absence of an electric field. The spontaneous polarization is a consequence of the positioning of the Ba^{+2}, Ti^{+4} and O^{-2} within the unit cell as in Fig. (1).

Under the ferroelectric curie temperature (120-130 °C), the unit cell of $BaTiO_3$ is tetragonal in which spontaneous polarization occurs as the titanium ions are displaced along the c-axis, but when $BaTiO_3$ is heated above this temperature, the unit cell became cubic (nonpolar phase) [3-5]. $BaTiO_3$ has a perovskite structure ($A^{+2}B^{+4}O_3$) in which (A= Ba^{+2}, B= Ti^{+4}). In this structure, Ba^{+2} coordinated by twelve oxygen ions, Ti^{+4} coordinated by 6 oxygen ions which form an octahedron as the structure in Fig. (1) [6]. This structure shows a cubic unit cell with large cation A on the corner, a smaller cation B in the body centers of the faces. $BaTiO_3$ was candidate for piezoelectric transducer applications and the ferroelectric multilayer ceramic capacitors (MLCCs) extremely important and widely used in many applications include capacitor, phonograph pickups, band pass filters, medical ultrasound, random access memories (RAMs), biocompatible, nanogenerators, etc. [7-9]. There are many studies that dealt with the preparation and study of $BaTiO_3$. Sareecha et al. [10] have studied the temperature dependence of dielectric constant for pure and Pb-doped $BaTiO_3$ ceramics. Shuvo et al. [11] have found that doping $BaTiO_3$ with 20% PbO leads to develop dielectric properties [11]. Zhang et al. [12] have elaborated the internal mechanism for high piezoelectric response of $Ba(Ti_{0.8}Zr_{0.2})O_3$-$(Ba_{0.7}Ca_{0.3})$ TiO_3. Kim and Song [13] have found that addition of MgO (0.2-1 wt.%) leads to increase the dielectric permittivity while it decreases with addition of Y_2O_3 (0.3-1.5 wt.%). Butee et al. [14] have prepared the $Ba_{1-x}Pb_xTiO_3$ and found that the Curie's temperature increases from 120 to 180 °C for x=0.15. Kadira et al. [15] have studied the effect of Ca^{+2} ion (x=0.01-0.1) on ferroelectric properties of $Ba_{1-x}Ca_xTiO_3$ and they found that the maximum Curie's temperature is at x=0.05. Islam et al. [16] have studied the effect of Mn^{+4} ions on the dielectric, microstructural properties of $BaMn_xTi_{1-x}O_3$ (x=0.0-0.04).

The aim of this work is to indicate and verify that whether the radius of the ion added to the base ion in the (A-site=Ba^{+2}) and (B-site=Ti^{+4}). In other words, the average ionic radius has an effect on ferroelectric Curie's temperature. Note that there are articles have shown that the ionic radius $\langle r_{A\text{-site}} \rangle$ of A-site ions affects strongly the Curie's temperature [17].

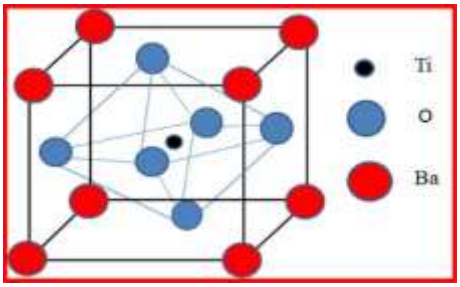

(a)

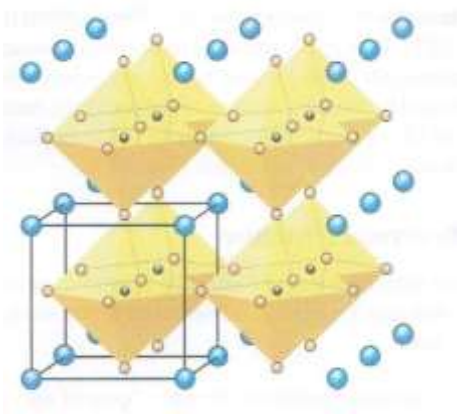

(b)

Fig. (1) (a) Structure of perovskite ABO_3 unit cell structure of $BaTiO_3$, (b) Perovskite structure as connected network of octahedral

2. Experimental Part

After performing the processes of weighing the used compounds according to the proportions mentioned in table (2), in which the mole ratio for both $BaCO_3$ and TiO_2 used in this work was [1:1] according to [18,19].

Table (1) Chemical compounds used in this work

No.	Compound	Origin	Purity (%)	Impurities (%)
1	TiO_2	BDH Chemicals Ltd (England)	98	Fe (0.5) L.I (0.5)
2	ZrO_2		98	HCl (0.005) Fe (0.002)
3	PbO (analar)		99	
4	CoO (black)			
5	$BaCO_3$	Riedel-De Haen (Germany)	99	Ca (0.01) Fe (0.001) Cl (0.005) NO_3 (0.005)
6	MnO_2		95	
7	SiO_2		99.51	
8	$CaCO_3$	Panreac Quimica SA (Spain)		

The wet mixing process was performed by using magnetic stirrer with heating at 70 °C after adding distilled water to the beakers containing prepared powders for a better reaction process. The mixing process lasted for 1 hour. After that, these beakers were placed in the oven at 150 °C for 2 hours to dry the samples. Then, these samples were grinded using a gate mortar for more homogeneity, and to check the prepared phase, samples were examined by yhe x-ray diffraction (XRD) technique using Philips PW 1316/90, single pen recorder (Cu K_α Target). After that, the samples were calcined in a muffle furnace at 1200 °C for 2 hours at heating rate of 8 °C/min. The calcined samples were strongly grinded using ball milled process to get the smallest grain size. The samples were placed in a cylindrical container with two stainless steel balls in which the crushing process holder is performed after placing the container on a vibrating stand for 2 hours.

Then, the crushed samples were pressed using hydraulic press as discs with diameter of 2 cm and thickness of 3-5 mm as shown in Fig. (2). For a coherent and regular shape, the PVA binder was used. The discs were sintering at 1200 °C for 2 hours at heating rate of 6 °C/min after remaining at 500 °C for 30 minutes to expel the binder and to prevent the cracks that led to damage the discs.

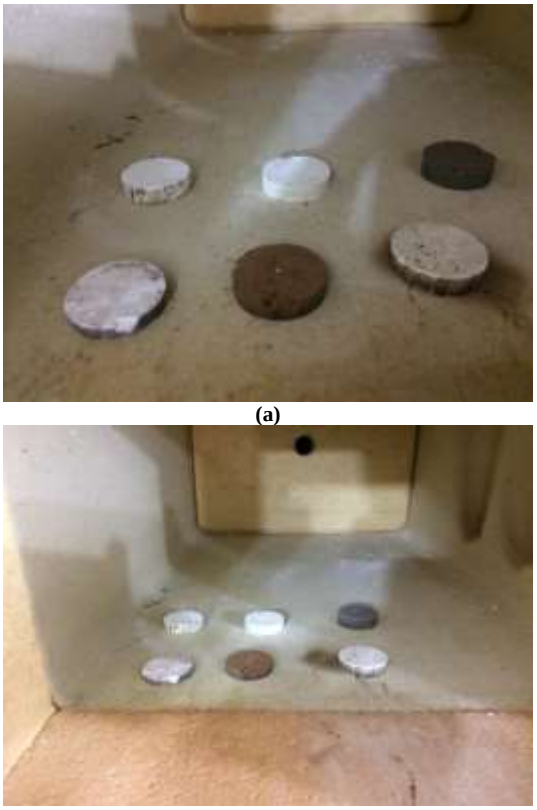

(a)

(b)

Fig. (2) Discs of prepared samples with 3-5mm thickness and 20mm diameter (in muffle furnace)

The grain size of samples were calculated depending on the XRD patterns using Scherrer's equation:

$$D = \frac{K\lambda}{\beta \cos\theta} \quad (1)$$

where D is mean crystallite size, K is Scherrer's constant, λ is diffraction wavelength, and β is the full-width at half-maximum (FWHM)

To calculate the dielectric constant versus temperature, determination of Curie's temperature from the Eq. (2) was used after measuring the electrical capacitance of the samples by using RCL-Meter (PM6303) at frequency of 20 Hz and electrical oven as a source of temperature.

$$\varepsilon_r = \frac{C\,d}{\varepsilon\,A} \quad (2)$$

here, C, d, A and ε represent the capacitance, thickness of samples, surface area of capacitors, and space permittivity (8.85×10^{-12}F/m), respectively

3. Results and Discussion

Figures (3) to (9) show the XRD patterns of $BaTiO_3$, $Ba_{0.85}Pb_{0.15}TiO_3$, $Ba_{0.85}Ca_{0.15}TiO_3$,

$Ba_{0.85}Co_{0.15}TiO_3$, $BaZr_{0.15}Ti_{0.85}O_3$, $BaSi_{0.15}Ti_{0.85}O_3$, $BaMn_{0.15}Ti_{0.85}O_3$, respectively. Figure (3) shows the good growth of the $BaTiO_3$ phase with the appropriate intensity of the main characteristic peaks of this phase namely [100], [101], [111], [002], [200], [201], [211], [202], [220], [301], [310] at 2θ=22.317°, 31.705°, 39.060°, 45.150°, 45.510°, 50.820°, 56.356°, 65.960°, 66.242°, 74.620°, and 75.230°. In addition, no impurities were found in this phase and the calcination at 1200 °C for 2 hours is appropriate to prepare $BaTiO_3$ phase in BaO-TiO_2 by using solid state reaction method.

Figures (4) and (5) also show good growth of the $Ba_{0.85}Pb_{0.15}TiO_3$ and $Ba_{0.85}Co_{0.15}TiO_3$ phases with no observed characteristic impurities except of the small intensity peak at 2θ=29.170° that belongs to PbO compound in Fig. (2). In Fig. (6), two peaks can be observed with distinguished intensities as they belong to CaO compound. This indicates the need to raise the calcination temperature to more than 1200 °C, and the evidence is that the phase growth has not been healed as required.

Figures (7), (8) and (9) also show good growth of $BaZr_{0.15}Ti_{0.85}O_3$, $BaMn_{0.15}Ti_{0.85}O_3$ and $BaSi_{0.15}Ti_{0.85}O_3$, respectively, with no observed characteristic impurities except in Fig. (5) at 2θ= 28.830° that belongs to ZrO_2 (JCPDS, 42-1164), and in Fig. (6) at 2θ=26.350° that belongs to MnO_2, and in Fig. (7) at 2θ=29.020° that belongs to SiO_2 (JCPDS, 40-1498).

Tables (2) and (3) show the crystal dimensions (*a*, *c*, *c/a*) and average crystallite size of prepared groups. By looking at tables (2) and (4), it can be found that the ratio *c/a* increases with decreasing average ionic radius of the site A in the structure of perovskites ABO_3 except for the group (4) where it remains relatively constant. As for the B site, there is no fixed relationship was found between the average ionic radius and the value of *a*, while the *c/a* ratio is greatly affected by the average ionic radius, as it increases with its increase and decreases with its decrease.

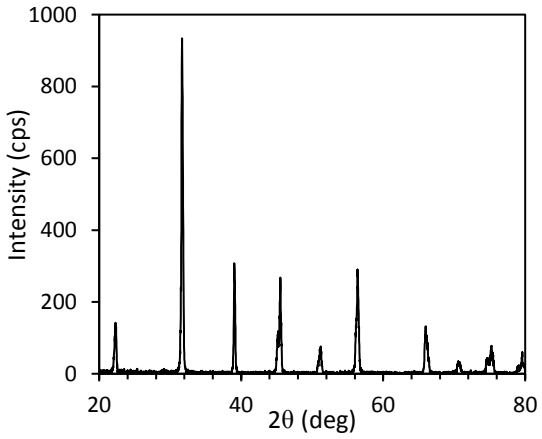

Fig. (3) XRD pattern of $BaTiO_3$ ceramic calcined at 1200°C for 2 hrs

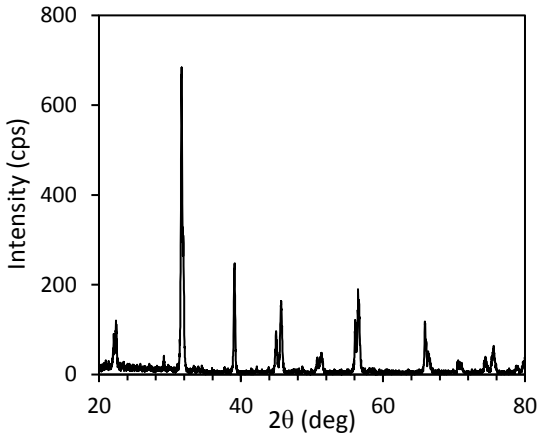

Fig. (4) XRD pattern of $Ba_{0.85}Pb_{0.15}TiO_3$ ceramic calcined at 1200°C for 2 hrs

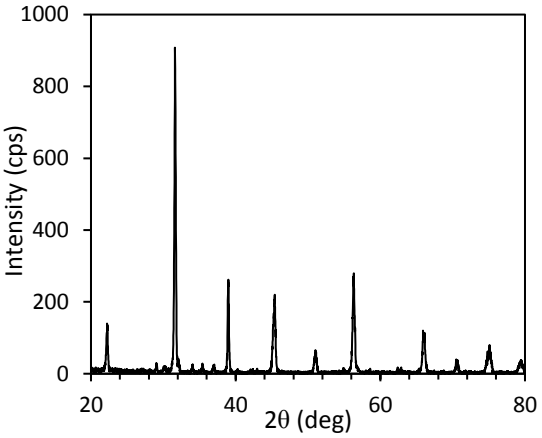

Fig. (5) XRD pattern of $Ba_{0.85}Co_{0.15}TiO_3$ ceramic calcined at 1200°C for 2 hrs

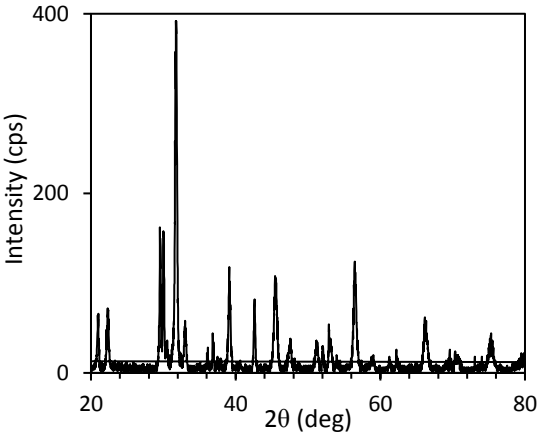

Fig. (6) XRD pattern of $Ba_{0.85}Ca_{0.15}TiO_3$ ceramic calcined at 1200°C for 2 hrs

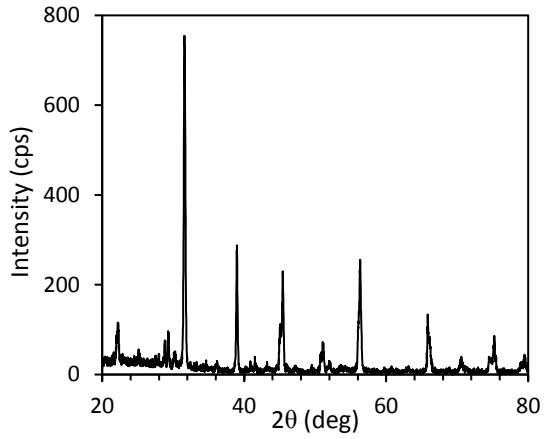

Fig. (7) XRD pattern of $BaZr_{0.15}Ti_{0.85}O_3$ ceramic calcined at 1200°C for 2 hrs

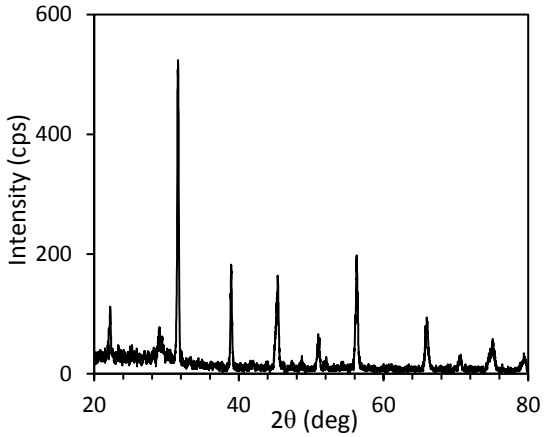

Fig. (8) XRD pattern of $BaSi_{0.15}Ti_{0.85}O_3$ ceramic calcined at 1200°C for 2 hrs

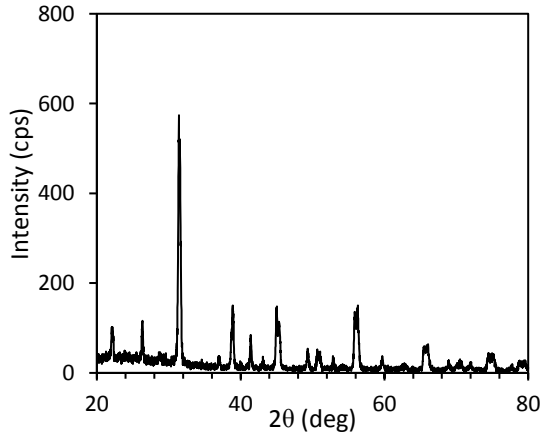

Fig. (9) XRD pattern of $BaMn_{0.15}Ti_{0.85}O_3$ ceramic calcined at 1200°C for 2 hrs

Figure (10) shows that the dielectric constant increases with increasing temperature at different rates from room temperature to temperatures close to Curie's temperature. This behavior is similar for all the prepared groups except for the group $Ba_{0.85}Co_{0.15}TiO_3$, where it is clearly seen that it is more stable in its dielectric constant within the thermal range 60-90 °C. Also, it is note that upon reviewing the radii of the ions that were compensated at the two sites A and B in the composition of perovskites ABO_3 (table 2).

Table (2) The crystal dimensions of groups

No.	Material	a (Å)	c (Å)	c/a
1	$BaTiO_3$	3.982	4.012	1.0075
2	$Ba_{0.85}Pb_{0.15}TiO_3$	3.980	4.030	1.0125
3	$Ba_{0.85}Ca_{0.15}TiO_3$	3.971	4.023	1.0131
4	$Ba_{0.85}Co_{0.15}TiO_3$	3.980	4.009	1.0073
5	$BaZr_{0.15}Ti_{0.85}O_3$	3.996	4.028	1.0080
6	$BaSi_{0.15}Ti_{0.85}O_3$	3.996	4.006	1.0025
7	$BaMn_{0.15}Ti_{0.85}O_3$	3.995	4.013	1.0045

Table (3) Crystallite size of prepared groups

No.	Material	Crystallite size (nm)	Average crystallite size (nm)
1	$BaTiO_3$	252 - 335	293.5
2	$Ba_{0.85}Pb_{0.15}TiO_3$	388 - 407	397.5
3	$Ba_{0.85}Ca_{0.15}TiO_3$	234.91 - 266.5	250.70
4	$Ba_{0.85}Co_{0.15}TiO_3$	330 - 396	363
5	$BaZr_{0.15}Ti_{0.85}O_3$	356 - 374	365
6	$BaSi_{0.15}Ti_{0.85}O_3$	330 - 388.04	359.02
7	$BaMn_{0.15}Ti_{0.85}O_3$	213.23 - 374.6	293.915

Table (4) The groups prepared in this work

No.	Compositions	$<r_{A\text{-site}}>$	$<r_{B\text{-site}}>$
1	$BaTiO_3$	1.61	0.605
2	$Ba_{0.85}Pb_{0.15}TiO_3$	1.592	
3	$Ba_{0.85}Ca_{0.15}TiO_3$	1.569	
4	$Ba_{0.85}Co_{0.15}TiO_3$	1.480	
5	$BaZr_{0.15}Ti_{0.85}O_3$		0.622
6	$BaSi_{0.15}Ti_{0.85}O_3$		0.574
7	$BaMn_{0.15}Ti_{0.85}O_3$		0.593

It was found that the decrease in the average ionic radius leads to a clear and large decrease in the dielectric constant at Curie's temperature, while increasing the average of the ionic radius at the site B leads to an increase in the value of the dielectric constant at Curie's temperature, as in the case when the relative substitution of Zr^{+4} ion instead of Ti^{+4} in the $BaZr_{0.15}Ti_{0.85}O_3$ group. Although, this cannot be generalized in absolute terms only after many appropriate experiments. The effect of the difference in the ionic radius for example between Zr^{+4} and Ti^{+4} ions in $BaZr_{0.15}Ti_{0.85}O_3$ group lead to octahedral oxygen distortion. This can be generalized to the rest of the prepared groups and it is believe that this may have the largest role in changing the values of the dielectric constant and Curie's point.

4. Conclusions

In concluding remarks, the temperature of 120 °C for 2 hours is suitable for preparing $BaTiO_3$. The effect of the average ionic radius on the displacement rate of the main peaks of the prepared compound can be observed. The occurrence of a creep and a shift in the direction of the decrease in the 2θ value of the main peaks, especially when the value of the average ionic radius changes in the B-site where we find the large relative displacement of the (110) peak of the groups ($BaZr_{0.15}Ti_{0.85}O_3$, $BaSi_{0.15}Ti_{0.85}O_3$, $BaMn_{0.15}Ti_{0.85}O_3$). To develop a comprehensive

general relationship linking the average ionic radius at the A,B sites in the composition of perovskites and between the crystal structure, its dimensions and the granular size, we must discuss and take into account other factors related to the physical and structural properties of the ion or the added oxide, the most important of which is the melting point. The average ionic radius at the A,B sites plays a large and clear role in determining the values of the dielectric constant and Curie temperature in perovskites.

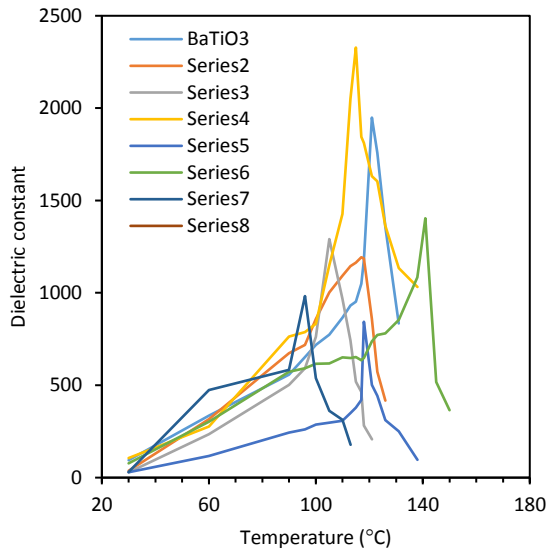

Fig. (10) Dielectric constant of prepared groups vs. temperature at 20 Hz, Series 2: $BaMn_{0.15}Ti_{0.85}O_3$, Series 3: $BaSi_{0.15}Ti_{0.85}O_3$, Series 4: $BaZr_{0.15}Ti_{0.85}O_3$, Series 5: $Ba_{0.85}Ca_{0.15}TiO_3$, Series 6: $Ba_{0.85}Pb_{0.15}TiO_3$, Series 7: $Ba_{0.85}Co_{0.15}TiO_3$

References

[1] J.C. Burffoot, **"Ferroelectrics, An Introduction to The Physical Principles"**, D. zan Nostrand Co. Ltd. (1967).

[2] M. Singh et al., "Synthesis and Characterization of Perovskite Barium Titanate Thin film and its Application as LPG sensor", J. Sen. Actuat., (2017) 1170-1178.

[3] K. Uchino, **"Ferroelectric Devices"**, 2nd ed., CRC Press, Taylor & Francis Group (2009).

[4] M.B. Smith et al., "Crystal Structure and The Paraelectric-to-Ferroelectric Phase Transition of Nanoscale $BaTiO_3$", J. Am. Chem. Soc., (2008) 6956-6963.

[5] P. Groen and J. Holterman, **"An Introduction to Piezoelectric Materials and Applications"**, Stiching Applied Piezo, Netherlands (2013).

[6] P. Groen and J. Holterman, **"An Introduction to Piezoelectric Materials and Applications"**, Stiching Applied Piezo, Netherlands (2012).

[7] K.R. Kambale, A.R. Kulkarni and N. Venkataramani, "Synthesis of Barium Titanate Powder Using Nanosized Titania", Int. J. Innov. Res. Sci. Eng. Technol., 3(6) (2014).

[8] S. Riaz et al., "Barium titanate films for electronic applications: structural and dielectric properties", Surf. Rev. Lett., 15(3) (2008) 237-244.

[9] M. Acosta et al., "$BaTiO_3$-based piezoelectrics: Fundamentals, current status, and perspectives", Appl. Phys. Rev., 4 (2017).

[10] N. Sareecha et al., "Fabrication and electrical investigations of Pb-doped $BaTiO_3$ ceramics", Mater. Chem. Phys. 193 (2017) 42-49.

[11] S.N. Shuvo, S. Saha and M. Rahman, "Dielectric and microstructural properties of PbO doped $BaTiO_3$", Int. J. Innov. Sci. Mod. Eng., 3(8) (2015).

[12] Y. Zhang, H. Sun and W. Chen, "A brief review of $Ba(Ti_{0.8}Zr_{0.2})O_3$-$(Ba_{0.7}Ca_{0.3})TiO_3$ based lead-free piezoelectric ceramics: past, present and future perspectives", J. Phys. Chem. Solids, 114 (2018) 207-219.

[13] H.D. Kim and J.T. Song, "The dielectric and electrical properties of a X7R multilayer ceramic capacitor", J. Cer. Process. Res., 12(3) (2011) 322-326.

[14] S. Butee et al., "Significant improvement in curie temperature and piezoelectric properties of $BaTiO_3$ with minimum Pb addition", J. Asian Ceram. Soc., 7(4) (2019) 407-416.

[15] L. Kadira, A. Elmesbahi and S. Sayouri, "Dielectric study of calcium doped barium titanate $Ba_{1-x}Ca_xTiO_3$ ceramics", Int. J. Phys. Sci., 11(6) (2016) 71-79.

[16] S. Islam et al., "Structural, dielectric and electric properties of manganese-doped barium titanate", Int. J. Nanoelectro. Mater., 11(4) (2018) 419-426.

[17] A. Berenov, F. Le Goupil and N. Alford, "Effect of ionic radii on the curie temperature in $Ba_{1-x-y}Sr_xCa_yTiO_3$ compounds", Sci. Rep., DOI:10.1038/srep28055 (2016).

[18] X. Liu et al., "Phase equilibria and thermodynamic evaluation of BaO-TiO_2-$YO_{1.5}$ system", J. Euro. Ceram. Soc., 38 (2018) 5430-5441.

[19] S. Lee and C. Randall, "Modified phase diagram oxide -titanium dioxide system for the ferroelectric barium titanate", J. Am. Ceram. Soc., 90(8) (2007) 2589-2594.

[20] A. Elbasset et al., "Influence of Zr on structure and dielectric behavior of $BaTiO_3$ ceramics", Indian J. Sci. Technol., 8(13) (2015). doi: thi0.17485/ijst/2015

IRAQI JOURNAL OF APPLIED PHYSICS
Vol. 17, No. 2, April-June 2021, p. 10

Raman Spectroscopy: New Strategy of Evaluating Metastatic Risk in Breast Cancer

Rebecca Ingle

Cancer diagnosis and treatment is often a race against time to ensure the best possible outcomes for the patient. A new study, published on the *bioRxiv preprint server, gives us one new tool for the rapid diagnosis and analysis of tumors by making use of Raman spectroscopy.[1]**

What is Raman Spectroscopy?

Raman spectroscopy is a workhorse technique in chemical identification and quantification. It is sensitive to the frequencies at which the chemical bonds in a molecule or material oscillate. As these frequencies are dependent on the masses of the atoms and the strengths of the bonds between them, these frequencies provide a unique fingerprint of the molecule that can be used for identification.

The Research

The US-based team, led by researchers at John Hopkins University, has developed a characterization method using Raman spectroscopy that allows them to identify the metastatic phenotype of a tumor – important information that can help identify how a tumor will continue to grow and progress. While Raman spectroscopy has already been used to investigate a range of biomedical problems, including tumor compositions, this was the first time it had been used to profile tumor phenotypes specifically.

Using a portable Raman instrument, the team made use of the unique fingerprints of the molecular species contributing to each phenotype to distinguish subtle changes in different tumor phenotypes in breast cancer cells from mice. Such cells are an excellent and widely used model for human cancers. These small differences that arise because of different gene expressions in tumors are key to the metastatic potential of a tumor, or how easily it will grow and spread.

Key to the success of this analysis strategy was the use of machine learning that meant the information recorded by the Raman instrument could be analyzed in an automated way. The team grouped potential tumor types into several categories and tried to classify them depending on their growth potential and current stage of development. They used five of the most unique spectral features in each Raman spectrum to classify the tumors to analyze the biomolecular content of each tissue sample.

After training the models, the team found that their approach was not just capable of differentiating between different tumor phenotypes, but also of differentiating between tumors that had undergone phenotype switching from natural metastasis or gene silencing experiments.

Given that metastasis to other parts of the body is one of the major causes of death from breast cancer, having a rapid diagnostic tool that can provide information on the metastasis stage and risk of tumors is a powerful asset for improving patient outcomes. Being able to identify what happens in tumors at a molecular level and how this changes during their growth processes is also invaluable information for understanding the fundamental science behind tumor development and for paving the way for new treatment approaches.

One of the advantages of using Raman spectroscopy for such diagnosis, as well as its excellent spectral sensitivity, is that this is a label-free technique that minimizes the need for sample preparation. Once the tumors had been excised, they were snap-frozen and then thawed in a saline buffer solution prior to measurements. For other diagnostic techniques, such as fluorescence microscopy, sample labeling is often an essential part of the process and there are some concerns that the use of labels can distort local environments during measurements.

The portability of the spectrometer and the automation of the spectral analysis with this approach may mean that this analysis method could potentially be used for rapid metastatic risk profiling of tumors in 'live' settings, such as surgery, where additional sample preparation and time-consuming measurements are unfeasible.

***Important notice**

bioRxiv publishes preliminary scientific reports that are not peer-reviewed and, therefore, should not be regarded as conclusive, guide clinical practice/health-related behavior, or treated as established information.

References and Further Reading

1. S. Paidi et al., "Raman spectroscopy reveals phenotype switches in breast cancer metastasis" (2021).

IRAQI JOURNAL OF APPLIED PHYSICS
Vol. 17, No. 2, April-June 2021, pp. 11-14

Spectroscopic Study of Chromium-Doped Silicon Nitride Nanostructures Prepared by DC Reactive Magnetron Sputtering

Firas J. Kadhim[1]
Oday A. Hammadi[2]
Ahmed A. Anber[3]

[1] *Department of Physics, College of Science, University of Baghdad, Baghdad, Iraq*
[2] *Department of Physics, College of Education, Al-Iraqia University, Baghdad, Iraq*
[3] *Department of Physics, College of Science, Al-Karkh University, Baghdad, Iraq*

In this work, chromium ions (Cr^{3+}) were embedded in silicon nitride nanostructures prepared by dc magnetron sputtering technique. Chromium oxide (Cr_2O_3) and silicon nitride (Si_3N_4 or SiN) powders were milled and mixed with fluxes (Na_2O and CaO) and intermediate material (Al_2O_3). This mixture was melted in an electric melting furnace at 1200°C. The structural properties of the resulted glass-ceramic structure were investigated by x-ray diffraction (XRD) while its spectral characteristics were determined by Fourier-transform infrared (FTIR) and UV-visible spectroscopies. Emission spectroscopy was carried out as well. The XRD results showed that the Cr^{3+} ions were freed from the Cr_2O_3 and interstitially embedded in the silicon nitride structure as dopants. The XRD also confirmed the formation of chromium nitride (CrN) as a result of some chemical reactions induced by melting process. Spectral characteristics showed that the absorption spectrum of the Cr^{3+}-doped Si_3N_4 sample was shifted towards the longer wavelengths when compared to the absorption spectrum of the Cr^{3+}-doped Si_3N_4 sample. This shift is attributed to ligand field and charge transfer mechanisms.

Keywords: Magnetron sputtering; Silicon nitride; Glass ceramic; Chromium oxide
Received: 25 February 2021; **Revised:** 8 April 2021; **Accepted:** 15 April 2021

1. Introduction

Over the past years, the technological developments have created the need for developing new materials and processes that can better fit the requirements for advanced applications. Silicon nitride is one of the most attractive advanced ceramic materials for structural applications due to its excellent mechanical properties, either at ambient or elevated temperatures [1]. Although several techniques for sintering silicon nitride are now available, most of them still require liquid phase formation to confer the ceramic high-density level [2]. Silicon nitride ceramics are generally used in high temperature oxidizing environments. Consequently, it is important to investigate the oxidation induced changes in the mechanical properties of these materials [3]. The effect of oxidation on the room, and high-temperature strength and fracture toughness of silicon nitride has been studied by numerous authors [4]. Although this scale protects the internal region of the material from the strong oxidation, the chemical and the phase compositions of the internal part change during the oxidation heat-treatment [5].

The effect of phase transformation occurred in the internal part during oxidation on the mechanical properties was also examined by few authors [3-5]. They found that internal stresses had developed due to crystallization of the inter-granular phase and that these stresses had a great influence on the room-temperature fracture toughness and strength of the material [5]. However, the effect of oxidation on other mechanical characteristics (e.g. hardness, elastic modulus) has not been studied [6,7].

Chromium is largely used in glasses for a broad range of applications. The redox state of Cr provides glasses specific light transmission properties, which are used, e.g., in packaging technology [8]. Cr(III) gives a green coloration in silicate glasses, whereas Cr(VI) imparts a yellow color and provides interesting thermos-chromic properties [9]. Cr(III) is also an efficient nucleating agent in oxide glasses and the redox state controls Cr solubility in glasses and melts [8,9]. Glass melting conditions are then adjusted to control Cr redox state, through an adequate choice of melting atmosphere or refining agents [10]. During the last years, many efforts for studying the effect of transition metal substitution on the formation ability of glasses have been conducted [11-14]. One of most important transition metals is chromium oxide, which has many applications in wide range of glasses [15,16].

The aim of the present work, which is part of the wider study on glassy and glass-ceramic from silicon nitride, is to study the effect of Cr_2O_3 on crystallization behavior of a two phases of silicon nitride Si_3N_4 and SiN.

2. Experimental Part

Silicon nitride nanostructures deposited on glass substrates using dc magnetron sputtering technique. The glass substrates were thoroughly cleaned with ethanol and distilled water before placed inside deposition chamber. The total gas pressure inside

chamber was kept constant at 0.36 mbar during deposition process. Two phases of silicon nitride (Si_3N_4 and SiN) were prepared. The discharge current was maintained at 30mA while the discharge voltage could be accurately varied (0-5kV). The deposition time was also varied to introduce the effect of different deposition rates on the thickness of prepared samples. More details on the dc magnetron sputtering system can be found elsewhere [17-21].

The powder of silicon nitride extracted from thin film samples was milled with powders of CaO and Na_2O as fluxes, Al_2O_3 as intermediate material and Cr_2O_3 as a coloring factor. The powders were milled in a planetary type alumina ball mill. The compositions of all starting materials are given in Table (1). The weighed materials were dried in oven at 110°C, introduced to blender for 30 min to produce homogeneous composition then put in an oven at 110°C for 24 hours to eliminate the humidity. The mixture was then placed in a graphite crucible and then inside an electric melting furnace (Mario Demaio) with heating poles made of carbon. The furnace temperature was increased automatically up to 1200 °C and each sample was kept inside the furnace for 2 hours at this temperature. The sample was manually mixed using long tongs every 20 min to ensure homogeneous melting process as well as to remove any bubbles might exist through the mixture.

Table (1) The composition of the prepared glass ceramic

Sample	Ceramic	Na_2O	CaO	Cr_2O_3	Al_2O_3
Si_3N_4-based	73%	9%	9%	4.5%	4.5%
SiN-based	73%	9%	9%	4.5%	4.5%

After melting period of 2 hours, the mold was casted in the same graphite crucible to obtained disk sample with a diameter of 2 cm and thickness of about 3 mm. The mold was placed inside a furnace heated up to 600°C for 2 hours to avoid the localized stresses inside the glass-ceramic composition. Such stresses may be induced by the sudden transfer of molten from melting to heat treatment temperature. The samples were dissolved by using HF to carry out the spectroscopic measurements.

3. Result and discussion

In Fig. (1), the XRD pattern of the Si_3N_4-based compound clearly shows distinct peaks belonging to CrN, SiO_2, CrO_3 and CrO_2 in addition to Si_3N_4. Oxygen was highly reduced from the Cr_2O_3 to form silicon dioxide (SiO_2). The oxidation of Si_3N_4 can thus be represented by the following equation [2,22]:

$$Si_3N_4 + 3O_2 \rightarrow 3SiO_2 + 2N_2 \qquad (1)$$

Also, the nitride ions can react with the chromium ions provided by the Cr_2O_3 to form CrN. Chromium in its 3^+ state forms a large number of complexes, particularly when nitrogen is the donor atom. The effect of Cr_2O_3 alone on the oxidation of Si_3N_4 can be represented by the following equation [2,22]:

$$Si_3N_4 + 2Cr_2O_3 \rightarrow 3SiO_2 + 4CrN \qquad (2)$$

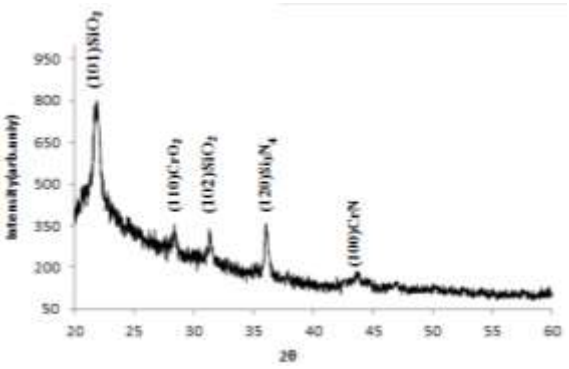

Fig. (1) The XRD patterns of Si_3N_4-based glass-ceramic sample

Figure (2) shows the XRD patterns of the SiN-based compound. Three peaks belonging to Si_3N_4, two peaks belonging to SiN, single peak belonging to Cr_2O_3 and single peak belonging to SiO_2 are observed. The diffraction line attributed to CrN was observed as well, however, this peak was shifted to a higher angle due to the change in silicon nitride phase. The glass-ceramic is apparently polycrystalline structure. This result agrees with the results obtained by FTIR spectroscopy.

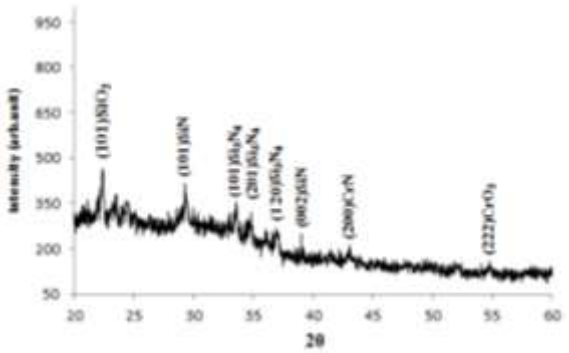

Fig. (2) The XRD patterns of SiN-based glass-ceramic sample

Figure (3) shows the results of FTIR spectroscopy, which was carried out to identify the chemical bonding induced by the melting process. The absorption of the Cr–N bond was observed at the low-wavenumber region due to the decomposition of silicon nitride freeing nitrogen ions to bond with Cr ones to form CrN. The absorption of Cr-O bond was also observed at 600-650 cm^{-1}. The absorption peaks assigning the Si-N bond in both samples are observed within 900-1100 cm^{-1}. Another peak occurs at 760 cm^{-1} is related to symmetrical expansion of Si-O-Si.

Figure (4) shows the absorption spectrum of both Cr^{3+}-doped silicon nitride samples (Si_3N_4 and SiN). The absorption peak at 350 might attributed to the absorption of silicon nitride in ultraviolet region,

while the absorption peaks at 255, 545 and 700nm are characteristic for the Cr^{3+} ions. Apparently, the effect of silicon nitride structure, in which the chromium ions are embedded, is observed by the shift of absorption peak from 400nm in case of Si_3N_4 to 421nm in case of SiN. This shift is attributed to ligand field and charge transfer mechanisms.

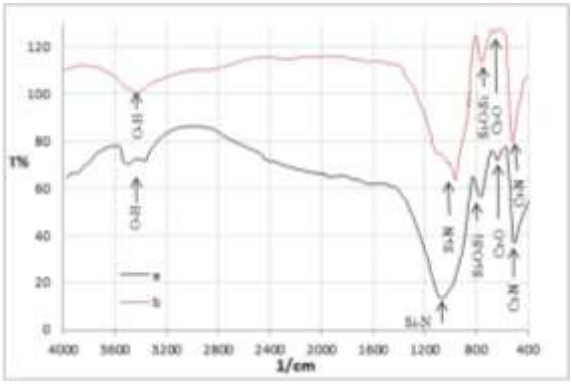

Fig. (3) The FTIR spectra of (a) Si_3N_4-based and (b) SiN-based glass-ceramic samples

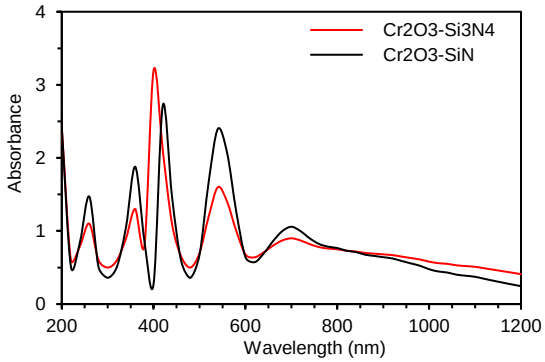

Fig. (4) The absorption spectra of Si_3N_4-based (red line) and SiN-based (black line) glass-ceramic samples

Figure (5) shows the emission spectra of 4.5 wt. % Cr^{3+}-doped silicon nitride samples excited by using 407nm radiation. There was no indication about the transition of Cr^{3+} in Fig. (5a), while the band located near 684.7 nm in Fig. (5b) might be attributed to the emission of the $^2E \rightarrow {}^4A_2$ transition of Cr^{3+} [23,24]. The broadening of the emission is probably caused by the electron-phonon coupling due to the phonon energy of Cr^{+3} [25,26], whereas the broadband emission may be ascribed to the transitions from some disordered Cr^{+3} ions [27].

Optical microscope images of the prepared glass-ceramics are shown in Fig. (6). Chromium oxide is well-distributed in the silicon nitride matrix. The microstructure shows two prevailing features; the first is no definite grain boundaries were detected but white regions due to melting of impurities in the glass-ceramic matrix. The green regions are the chromium oxide. The second feature is the small size of pores (dark regions) compared to the glassy regions of larger sizes.

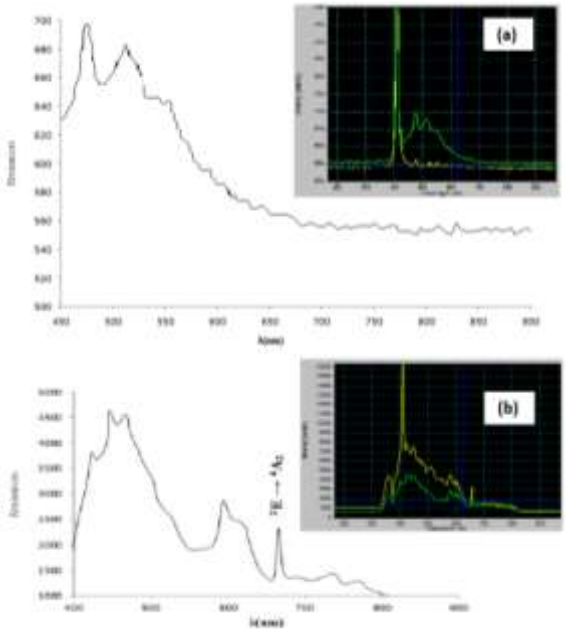

Fig. (5) The emission spectra of (a) Si_3N_4-based and (b) SiN-based glass-ceramic samples. In case of sample (b), a strong emission line is observed in the vicinity of 684.7 nm confirming the activity of Cr^{3+} embedded in silicon nitride structure

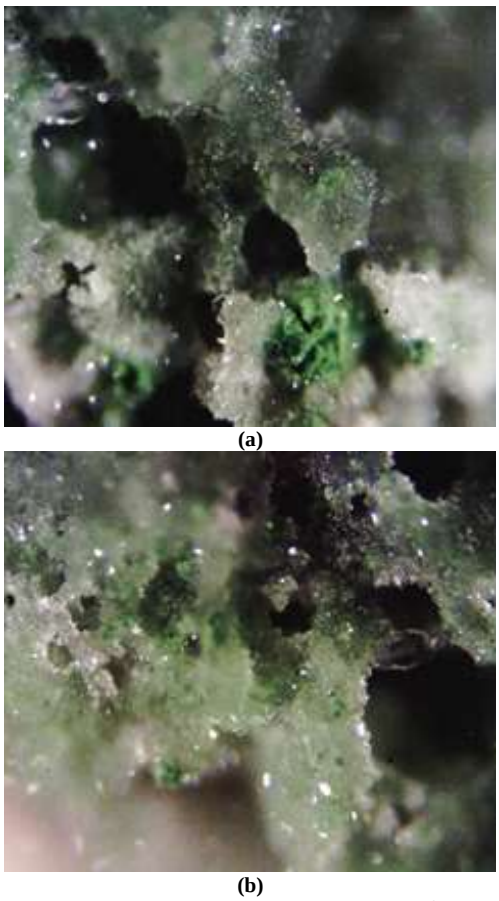

(a)

(b)

Fig. (6) The optical microscope images (x250) of (a) Si_3N_4-based and (b) SiN-based glass-ceramic samples

4. Conclusion

According to the obtained results, the compositions of silicon nitride and chromium oxide can be successfully melted at 1200°C by adding CaO and Na_2O as fluxes. The formation of chromium nitride has confirmed the decomposition of some silicon nitride molecules due to melting process to free nitrogen ions those bond with chromium ions freed from chromium oxide leaving enough oxygen to bond with silicon atoms to form silicon dioxide. The absorption of Cr^{3+}-doped silicon nitride glass-ceramic depends on the structure of ceramic as a shift can be done in an absorption peak from 400 to 421nm when replacing Si_3N_4 by SiN. A transition of $^2E \rightarrow {}^4A_2$ in Cr^{3+} at 684.7 nm was confirmed by the emission spectrum.

References

[1] O.A. Hammadi, M.K. Khalaf, F.J. Kadhim, "Silicon Nitride Nanostructures Prepared by Reactive Sputtering Using Closed-Field Unbalanced Dual Magnetrons", Proc. IMechE, Part L, J. Mater.: Design and Applications, 231(5) (2017) 479-487.

[2] Ch. He, L. Wang and J. Wu, "Oxidation of Sintered Silicon Nitride", J. Mater. Sci., 28(18) (1993) 4829-4834.

[3] Y. Ukyo, "The effect of a small amount of impurity on the oxidation of Si_3N_4 ceramics", J. Mater. Sci., 32(20) (1997) 5483-5489.

[4] M.K. Cinibulk and H.-J. Kleebe, "Effects of oxidation on intergranular phases in silicon nitride ceramics", J. Mater. Sci., 28(21) (1993) 5775-5782.

[5] J. Gubicza et al., "Mechanical properties of oxidized silicon nitride ceramics", Mater. Sci. Eng. A, 259 (1999) 65-72.

[6] M.K. Cinibulk et al., "Amorphous Intergranular Films in Silicon Nitride Ceramics Quenched from High Temperatures", J. Am. Ceram. Soc., 76(11) (1993) 2801-2808.

[7] T. Ekström and M. Nygren, "SiAION Ceramics", J. Am. Ceram. Soc., 75(2) (1992) 259-276.

[8] R.H.M. Godoi et al., "Chromium-containing silica materials", J. Non-Cryst. Solids, 273(1) (2000) 36-40.

[9] R.H.M. Godoi et al., "Investigation of the systems silica and silica containing chromium in alcohol medium", J. Non-Cryst. Solids, 247(1-3) (1999) 141-145.

[10] P. Hrma et al., "Chromium Phase Behavior in a Multi-Component Borosilicate Glass Melt", J. Non-Cryst. Solids, 352(21) (2006) 2114-2122.

[11] Y. Long et al., "Effects of transition metal substitution on the glass-formation ability and magnetic properties of $Fe_{62}Co_{9.5}Nd_3Dy_{0.5}B_{25}$ glassy alloy", J. Appl. Phys., 91(8) (2002) 5227.

[12] H. Yang, X. Li and Y. Li, "The effect of various transition metals on glass formation in ternary La-TM-Al (TM = Co, Ni, Cu) alloys", J. Mater. Res., 26(8) (2011) 992-996.

[13] Z.P. Lu and C.T. Liu, "A new glass-forming ability criterion for bulk metallic glasses", Acta Mater, 50(13) (2002) 3501-3512.

[14] D.B. Miracle, W.S. Sanders and O.N. Senkov, "The influence of efficient atomic packing on the constitution of metallic glasses", Philos. Mag., 83(20) (2003) 2409-2428.

[15] S.R. Bhagavatula and R. Komanduri, "On chemomechanical polishing of Si_3N_4 with Cr_2O_3", Philosoph. Mag. A, 74(4) (1996) 1003-1017.

[16] B. Mirhadi and B. Mehdikhani, "The effect of chromium oxide on optical spectroscopy of sodium silicate glasses", J. Optoelectron. Adv. Mater., 13(9) (2011) 1067-1070.

[17] O.A. Hammadi et al., "Operation Characteristics of a Closed-Field Unbalanced Dual-Magnetrons Plasma Sputtering System", Bulg. J. Phys., 41(1) (2014) 24-33.

[18] M.K. Khalaf, F.J. Kadhim and O.A. Hammadi, "Effect of Adding Nitrogen to the Gas Mixture on Plasma Characteristics of a Closed-Field Unbalanced DC Magnetron Sputtering System", Iraqi J. Appl. Phys. (IJAP), 10(1) (2014) 27-31.

[19] O.A. Hammadi, M.K. Khalaf, F.J. Kadhim, "Fabrication of UV Photodetector from Nickel Oxide Nanoparticles Deposited on Silicon Substrate by Closed-Field Unbalanced Dual Magnetron Sputtering Techniques", Opt. Quantum Electron., 47(12) (2015) 3805-3813.

[20] O.A. Hammadi, M.K. Khalaf, F.J. Kadhim, "Fabrication and Characterization of UV Photodetectors Based on Silicon Nitride Nanostructures Prepared by Magnetron Sputtering", Proc. IMechE, Part N, J. Nanoeng. Nanosys., 230(1) (2016) 32-36.

[21] O.A. Hammadi, "Characterization of SiC/Si Heterojunction Fabricated by Plasma-Induced Growth of Nanostructured Silicon Carbide Layer on Silicon Surface", Iraqi J. Appl. Phys. (IJAP), 12(2) (2016) 9-13.

[22] T.J. Harrington and A. Earnshawa, "The Chemistry of Transition Metals", Clarendon Press (Oxford) (1973) 36, 61-62.

[23] A.J. Wojtowicz, "Physics of Solid-State Laser Materials", Acta Physica Polonica A, 80(2) (1991) 193-205.

[24] F.A. Miller and C.H. Wilkins, "Infrared Spectra and Characteristic Frequencies of Inorganic Ions, Their use in qualitative analysis", Anal. Chem., 24(8) (1952) 1253-1294.

[25] N. Ollier et al., "Influence of impurities on Cr^{3+} luminescence properties in Brazilian emerald and alexandrite", Euro. J. Mineralogy, 27(6) (2015) 783-792.

[26] P.D. Rack et al., "Eu^{+3} and Cr^{+3} doping for red cathodoluminescence in $ZnGa_2O_4$", J. Mater. Res., 16(5) (2001) 1429-1433.

[27] M. Grinberg, "Spectroscopic characterisation of disordered materials doped with chromium", Opt. Mater., 19(1) (2002) 37-45.

IRAQI JOURNAL OF APPLIED PHYSICS
Vol. 17, No. 2, April-June 2021, pp. 15-18

Effects of Solvent Properties on Absorption and Fluorescence Characteristics of Two Organic Dyes Used as Random Gain Media

Mohammed A. Hameed

Department of Physics, College of Science, University of Baghdad, Baghdad, IRAQ

In this work, the effects of solvent properties on the characteristics of absorption and fluorescence for two laser dyes was studied. Dyes used in this work include Coumarin 5400 and DCM, while the solvents include ethanol, methanol, acetone, propanol and chloroform. Coumarin 5400 dye shows sharp fluorescence peaks in the green band of visible region while the DCM dye shows relatively wide band within 590-630 nm. Therefore, the selection of any dye for random gain medium applications should be performed after determining the most appropriate solvent as the optimum fluorescence characteristics are obtained.

Keywords: Spectroscopy; Laser dyes; Fluorescence; Gain media
Received: 12 April 2021; **Revised**: 10 May 2021; **Accepted**: 17 May 2021

1. Introduction

The importance of organic dyes in the spectroscopic, environmental and industrial applications are drastically increased due to many recent uses appeared during the last two decades [1]. In spectroscopic and molecular physics, using such dyes as gain media represents one of the most featured applications [2]. One major type of lasers was known as dye lasers due to the type of active medium exhibiting the laser action [2-5].

Laser dye is an unsaturated hydrocarbon organic compound containing a mutual series of carbon atoms, with successive single and double bonds [6,7]. The chromophores in lasing compound molecules are an active group capable of absorbing ultraviolet and/or visible light (200-800nm) [8,9]. The main property of laser dyes is the possibility for tuning the frequency of laser oscillation, which makes it possible to change the wavelength of emitted laser radiation to a range of approximately 60 nm [10,11]. By using different dye, a wide range of laser wavelengths can be obtained [12].

The most recent type of dye lasers is the random laser whose active medium is characterized as random gain medium [13]. This type of dye lasers does not require the conventional amplification mechanism, known as optical resonator, instead, it employs the same organic dye medium containing some optically-active particles as scattering centers within the dye [14].

These scattering centers play the role of too many resonators inside the dye medium to achieve the required amplification of laser radiation [15]. As these particles are randomly distributed inside the dye medium, this gain medium is known as random gain medium [16]. Type of scattering (Rayleigh or Mie) is fundamentally determined by the particle size, therefore, the efficiency of light amplification process is accordingly dependent on particle size [17,18].

The absorption and fluorescence spectra of dyes generally differ from the atomic spectra by their wide and structureless bands of tens of nanometers [19,20]. The peak of fluorescence spectrum is shifted toward the longer wavelengths (red shift) as compared to that of the absorption spectrum. This is known as Stoke's shift [21,22]. Despite, there still an overlapping region between two spectra, which is attributed to a re-absorption process and consequently a re-emission (as fluorescence) can occur. This gives rise to the superposition of longer wavelengths of the absorption spectrum with shorter wavelengths of the fluorescence spectrum, thereby changing the shape of fluorescence spectrum and its quantum yield [23,24].

2. Experimental Work

The dye solutions was prepared by dissolving different molar concentrations of Coumarin 5400 and 4-Dicyanomethylene-2-methyl-6-p-diethylaminostyryl-4-H-pyran (shortly known as DCM) dyes (10^{-2}, 10^{-3}, $5x10^{-3}$, 10^{-4}, $5x10^{-4}$, 10^{-5} M) in different solvents (ethanol, methanol, acetone, propanol and chloroform). Absorption and fluorescence spectra were recorded to determine the optimum concentration and solvent.

The spectroscopic characteristics of the dye solutions were determined by a computer-controlled UV-Visible spectrophotometer (K-MAC SpectraAcademy SV-2100) in the spectral range 166-962 nm and the fluorescence spectra were recorded using an F96 Fluorescence

Spectrophotometer unit (Shanghai LengGuang Tech. Co., Ltd.) in the spectral range of 180-900 nm with a cw xenon lamp as the excitation source.

3. Results and Discussion

Figure (1) shows the absorption spectra of Coumarin 5400 dye solutions in different solvents in the spectral range 300-700 nm. It is clear that the dye solution in methanol shows the highest absorbance at 430 nm, while the dye solutions in acetone and chloroform show comparable absorbance and the dye solution in ethanol shows rather lower absorbance at the same wavelength (430 nm). The dye solution in propanol shows very low absorbance. These results are mainly attributed to the high polarity of methanol and acetone when compared to ethanol and chloroform, as shown in table (1), while the dye solution in propanol of the lowest polarity shows lower values of absorbance. Chloroform often contains ethanol as a preservative, and since ethanol has high solvent strength, small amounts may have a dramatic effect [25].

Another property of solvent should be considered is the solvent strength, which perhaps is the most widely recognized characteristic solvent property. The solvent strength parameter provides a quantitative measure of the relationship between solvent strength and the type of sorbent used. The absorbance of the dye solution in methanol clearly indicates the effect of solvent strength.

Table (1) Polarities and strengths of the solvents used in this work [25]

Solvent	Polarity	Solvent Strength	Refractive Index	UV Cutoff (nm)
Acetone	5.1	0.56	1.356	330
Chloroform	4.1	0.40	1.443	245
Ethanol	4.3	0.88	1.359	210
Methanol	5.1	0.95	1.326	190
Propanol	4.0	0.82	1.385	240

Figure (2) shows the fluorescence spectra of Coumarin 5400 dye solutions in different solvents excited by 405 nm radiation. All sample shows fluorescence peak within the green band of visible region (530-535nm). However, the dye solution in ethanol shows sharp peak at 532.8 nm and that in propanol shows slightly wider peak but around the same wavelength. The dye solutions in the other three solvents (methanol, acetone and chloroform) show relatively wide peak within 531-534 nm. As the dye solutions prepared in this work are required for random gain media, then the dye solutions in ethanol and propanol would be good candidates for such purpose. However, the fluorescence efficiency is low as the absorbance of both samples are reasonably lower than that of other three samples. Therefore, a compromise should be done to choose the most suitable sample for the required application.

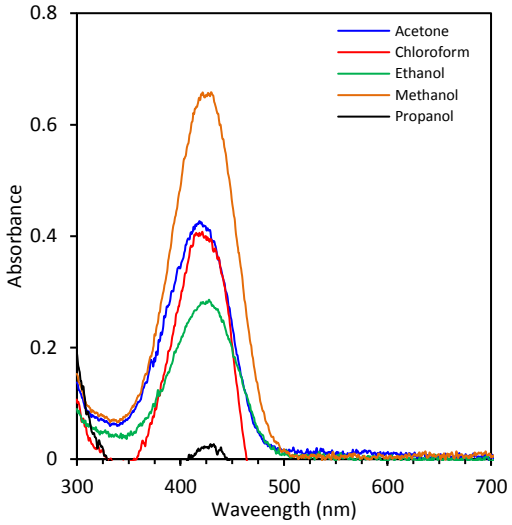

Fig. (1) Absorption spectra of Coumarin 400 dye solutions in different solvents

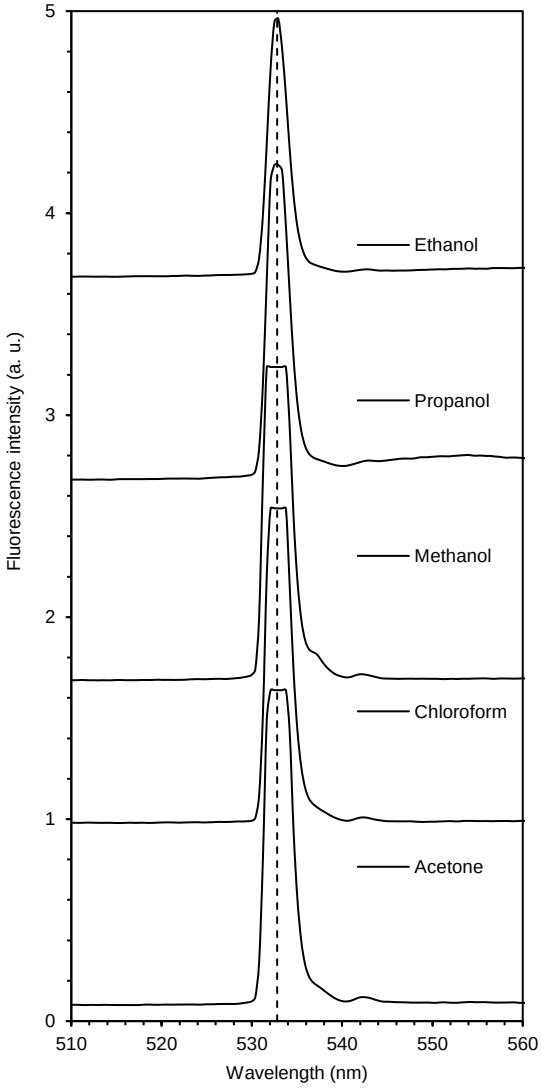

Fig. (2) Fluorescence spectra of Coumarin 400 dye solutions in different solvents using excitation wavelength of 405 nm

Four of the previous solvents were used to prepare DCM dye solutions to be compared with those of Coumarin 5400. The absorbance of dye solutions in acetone, chloroform, propanol and methanol are sorted from the highest to lowest with a red shift in the peak from 469 to 475 nm. Also, the DCM dye solutions in acetone, chloroform and propanol show higher absorbance than those of Coumarin 5400 in the same solvents. This behavior was different for the DCM dye solution in methanol as its absorbance is lower than 50% of absorbance of Coumarin dye solution in methanol. This results shows that the polarity and strength of the solvents are not highly effective as in the results of Coumarin dye solutions. However, the UV cutoff wavelength and refractive index of the solvent may have stronger roles in determining the absorption characteristics of the dye solution (see table 1).

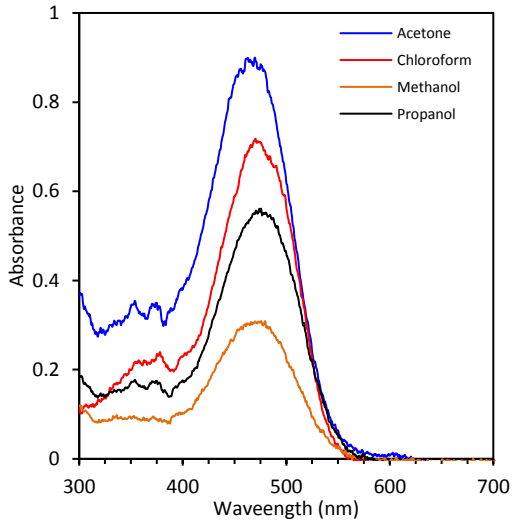

Fig. (3) Absorption spectra of DCM dye solutions in different solvents

The DCM dye solutions were excited by 532 nm radiation in order to record the fluorescence spectra. The dye solution in chloroform shows a relatively wide peak within 568-600nm. As well, the dye solutions in acetone and propanol show a peak at 610 nm, the dye solution in methanol shows a peak at 613 nm, and the dye solution in ethanol shows a peak at 614 nm. Therefore, this slight red shift ascribed to the combination of solvent properties listed in table (1), mainly, refractive index and polarity, as the dye solutions in chloroform and acetone show fluorescence peaks at shorter wavelengths as mentioned above.

An important observation on these spectra is the peak seen at 811-812 nm, which may make these dye solutions applicable in producing new laser action in the NIR region. However, the intensity of this peak is reasonably low in all samples.

Since no specific property of the solvent is thought to be the reason behind the results shown in Fig. (4), then the interaction between the solvent and dye molecules can be the most important parameter that governs the spectroscopic behavior of dye solution in each solvent.

The solvent-induced broadening of the spectral lines and bands arises primarily from the variation of the local environment of the chromophoric solute molecule in the condensed medium caused by the thermal motion of the surrounding solvent molecules [26].

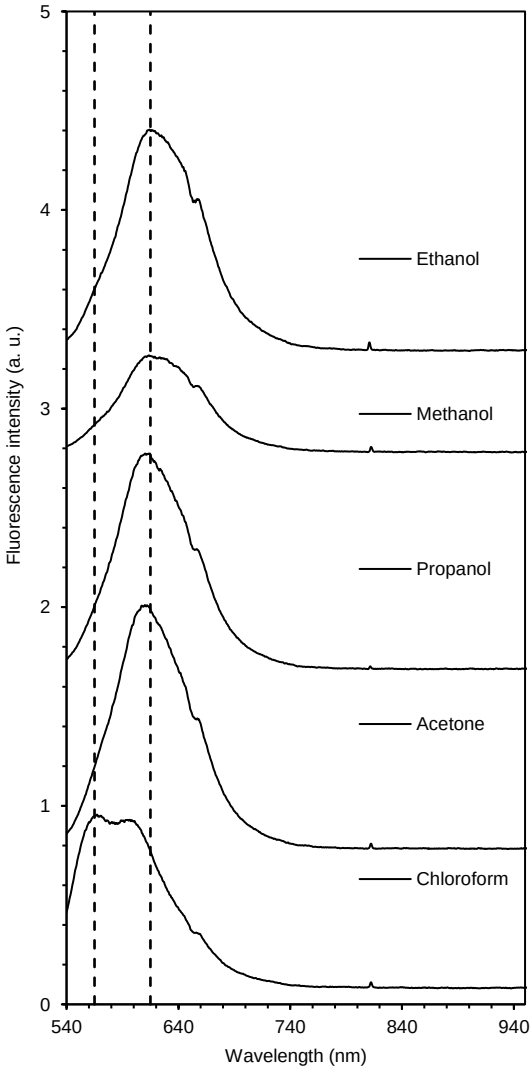

Fig. (4) Fluorescence spectra of DCM dye solutions in different solvents using excitation wavelength of 532 nm

4. Conclusion

In concluding remarks, the effect of solvent type on the absorption and fluorescence characteristics of two organic dyes (Coumarin 5400 and DCM) was determined and studied. The Coumarin 5400 dye shows sharp fluorescence peaks in the green band of visible region while the DCM dye shows relatively wide band within 590-630 nm. Therefore, the selection of any dye for random gain medium applications should be performed after determining the most appropriate solvent as the optimum fluorescence characteristics are obtained. This study

may motivate to study the effects of other solvents as well as their physical and chemical properties on the fluorescence characteristics of dyes used for the construction of random gain media.

References

[1] D.S. Wiersma, "The physics and applications of random lasers", Nature Physics, 4 (2008) 359-365.
[2] A. Ishimaru, "Wave propagation and scattering in random media", Academic Press, New York (1978) pp. 175-183.
[3] M.P. van Albada and A. Lagendijk, "Observation of weak localization of light in random medium", Phys. Rev. Lett. 55 (1985) 2692-2695.
[4] P.E. Wolf, G. Maret, E. Akkermans and R. Maynard, "Optical coherent backscattering by random media: an experimental study", J. Phys. France, 49 (1988) 63-75.
[5] P. Sebbah, C. Vanneste," Random laser in the localized regime", Phys. Rev. B, 66 (2002) 144-202.
[6] J. Andreasen, A.A. Asatryan, L.C. Botten, M.A. Byrne, H. Cao, L. Ge, L. Labonté, P. Sebbah, A.D. Stone, H.E. Türeci and C. Vanneste, "Modes of random lasers", Adv. in Optics and Photonics, 3(1) (2011) 88-127.
[7] R.C. Polson and Z.V. Vardeny, "Random lasing in dye-TiO_2 solution and π-conjugated polymer films", Physica B, 338 (2003) 219-223.
[8] D.S. Wiersma, M.P. van Albada and A. Lagendijk, "Random Laser?", Nature, 373 (1995) 203-204.
[9] S.A. Ramakrishna, "Mirror less lasing in random amplifying media", Bull. Indian Laser Assoc., 10-11(4) (2000) 28-33.
[10] H. Cao, Y.G. Zhao, S.T. Ho, E.W. Seeling, Q.H. Wang, and R.P.H. Chang, "Random laser action in semiconductor powder", Phys. Rev. Lett., 82(11) (1999) 2278-2281.
[11] S. Garcia-Revilla, M. Zayac, R. Balda, M. Al-Saleh, D. Levy and J. Fernandez, "Low threshold random lasing in dye-doped silica nano powders", Optics Express, 17(15) (2009) 13202-13215.
[12] J. Kitur, G. Zhu, M. Bahoura and M.A. Noginov, "Dependence of the random laser behavior on the concentrations of dye and scatterers", J. Optics, 12(2) (2010) 024009.
[13] Wei-Tang Li, Effect of sputtering-gas pressure on properties of silicon nitride films produced by helicon plasma sputtering, Thin Solid Films, 384, 46-52 (2001).
[14] M. Vila, D. Cáceres and C. Prieto, Mechanical properties of sputtered silicon nitride thin films, J. Appl. Phys., 94(12), 7868-7873 (2003).
[15] Gang Xu, Optical investigation of silicon nitride thin films deposited by r.f. magnetron sputtering, Thin Solid Films, 425, 196–202 (2003).
[16] S.A. Awan and R.D. Gould, Conductivity and dielectric properties of silicon nitride thin films prepared by RF magnetron sputtering using nitrogen gas, Thin Solid Films, 423, 267–272 (2003).
[17] Zh.Q. Yao, Studies of the composition, tribology and wetting behavior of silicon nitride films formed by pulsed reactive closed-field unbalanced magnetron sputtering, Nuclear Instrum. Meth. in Phys. Res., B242, 33–36 (2006).
[18] X. Zhang and C.P. Grigoropoulos, Thermal conductivity and diffusivity of free-standing silicon nitride thin films, Rev. Sci. Instrum., 66(2), 1115-1120 (1995).
[19] A. Batan, Characterisation of the silicon nitride thin films deposited by plasma magnetron, Surf. Interface Anal., 40, 754–757 (2008).
[20] M.A. Hameed and Z.M. Jabbar, "Optimization of Preparation Conditions to Control Structural Characteristics of Silicon Dioxide Nanostructures Prepared by Magnetron Plasma Sputtering", Silicon, 10 (2018) 1411-1418.
[21] B.K. Nasser and M.A. Hameed, "Structural Characteristics of Silicon Nitride Nanostructures Synthesized by DC Reactive Magnetron Sputtering", Iraqi J. Appl. Phys., 15(4) (2019) 33-36.
[22] B.K. Nasser and M.A. Hameed, "Narrow Emission Linewidth of Highly-Pure Silicon Nitride Nanoparticles in Different Dye Solutions as Random Gain Media", Nonl. Opt. Quant. Opt., accepted for publication (2020).
[23] Ru Xia et al., Surface modification of nano-sized silicon nitride with BA-MAA-AN tercopolymer, J. Appl. Polymer Sci., 107 (2008) 562-570.
[24] Olivier Debieu, Structural and optical characterization of pure Si-rich nitride thin films, Nanoscale Res. Lett., 8 (2013) 31.
[25] H. Günzler and A. Williams (editors), **"Handbook of Analytical Techniques"**, Wiley-VCH Verlag GmbH (Germany) (2001), p. 284, 335.
[26] G. Wypych (editor), **"Handbook of Solvents"**, ChemTec Publishing (Toronto, 2001), p. 643.

THE IRAQI JOURNAL OF APPLIED PHYSICS
EDITORIAL BOARD

COPYRIGHT RELEASE FORM
IRAQI JOURNAL OF APPLIED PHYSICS (IJAP)

We, the undersigned, the author/authors of the article titled

……
……
……
……
……
……
……

that is submitted to the Iraqi Journal of Applied Physics (IJAP) for publication, declare that we have neither taken part or full text from any published work by others, nor presented or published it elsewhere in any other journal. We also declare transferring copyrights and conduct of this article to the Iraqi Journal of Applied Physics (IJAP) after accepting it for publication.

The authors will keep the following rights:

1. Possession of the article such as patent rights.
2. Free of charge use of the article or part of it in any future work by the authors such as books and lecture notes after informing IJAP editorial board.
3. Republishing the article for any personal purposes of the authors after taking journal permission.

To be signed by all authors:

Signature:……..date: ……
Printed name: ……

Signature:……..date: ……
Printed name: ……

Signature:……..date: ……
Printed name: ……

Correspondence
address:……..……...
……
Address:……..……
……
Telephone:……..……..email: ……

Note: Complete and sign this form and mail it to the below address with your finally revised manuscript

The Iraqi Journal of Applied Physics
www.iraqiphysicsjournal.com
Email: info@iraqiphysicsjournal.com
Email: editor_ijap@yahoo.co.uk
Email: irq_appl_phys@yahoo.com

IRAQI JOURNAL OF APPLIED PHYSICS

Volume (17), Issue (2), April-June 2021

CONTENTS